Bull. Inst. Chem. Res., Kyoto Univ., Vol. 69, No. 2, 1991.

Intramolecular and Intermolecular Hydrogen Bondings of Poly(vinyl alcohol) in the Solid State

Shaohua Hu*, Fumitaka Horii**, and Hisashi Odani**

Received July 1, 1991

The intramolecular and intermolecular hydrogen bondings have been examined for poly(vinyl alcohol) (PVA) films with different tacticities by CP/MAS ^{13}C NMR spectroscopy and a statistical calculation. The CH resonance line splits into a triplet, lines I, II, and III, due to the formation of two, one, and no intramolecular hydrogen bond(s) in the triad sequences for the crystalline and noncrystalline components, respectively. The integrated fractions of lines I, II, and III have been statistically calculated using a structure model based on the crystal structure proposed by Sakurada *et al.*, where the intramolecular and intermolecular hydrogen bonds are formed at certain probabilities for all possible triad-tetrad or triad-triad pairs in the neighboring two chains. The observed fractions, which are determined by the lineshape analysis of the CH triplet, are in good accord with the calculated fractions for different PVA samples. On the basis of these results, the characteristic intramolecular and intermolecular hydrogen bondings are discussed for the crystalline and noncrystalline components of almost atactic PVA films in the dried or hydrated state as well as for the crystalline components of dry syndiotacticity-rich and isotacticity-rich PVA films.

KEY WORDS: High-Resolution Solid-State ^{13}C NMR / Poly(vinyl alcohol) / Crystal Structure / Hydrogen Bonding / Effect of Water / Tacticity/

INTRODUCTION

High-resolution solid-state ^{13}C NMR spectroscopy, which is frequently abbreviated as cross polarization/magic angle spinning (CP/MAS) ^{13}C NMR spectroscopy, is very powerful in characterizing the structure and molecular motion of crystalline and noncrystalline regions of different polymers. We have already investigated the structure of the crystalline and amorphous regions as well as the interfacial region, which may be defined as a transition region between the crystalline and noncrystalline regions, for isothermally crystallized polyethylene,[1] uniaxially oriented polyethylene,[2,3] super-drawn polyethylene,[4] high-pressure crystallized polyethylene,[5] isothermally crystallized polypropylene[6] and poly(tetramethylene oxide).[7] Similar ^{13}C NMR analyses were also applied to the detailed characterization of the crystalline and noncrystalline structures of native cellulose,[8-12] amylose,[13] and dextran,[14] and of the molecular motion of poly(methyl methacrylate)s with different tacticities,[15] terephthalic-acid polyesters with different lengths of the methylene sequences,[16,17] and Si containing polyacetylene derivatives[18] in the glassy and rubbery states.

* 胡紹華: On leave from Shanghai College of Petrochemical Technology, Jinshanwei, Shanghai, PRC.

** 堀井文敬, 小谷壽: Laboratory of Fundamental Material Properties, Institute for Chemical Research, Kyoto University, Uji, Kyoto 611, Japan.

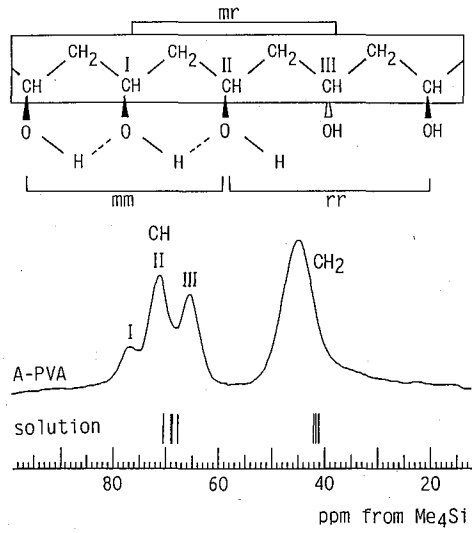

Fig. 1 50 MHz CP/MAS ^{13}C NMR spectrum of almost atactic PVA films (A-PVA) measured at room temperature and a schematic representation of the intramolecular hydrogen bonding in the triad sequences.

The information about the hydrogen bonding associated with OH groups is also obtained by CP/MAS ^{13}C NMR spectroscopy. In solid poly(vinyl alcohol) (PVA),[19-21] as shown in Figure 1, the CH resonance line splits into a triplet with the splitting width of about 5 ppm, which is much larger than the width of the triplet induced by the different triad tacticities, *mm*, *mr*, and *rr* in the solution-state spectrum shown as a stick-type spectrum in Figure 1. Such a large splitting is ascribed to the formation of the intramolecular hydrogen bonding in the *mm* and *mr* sequences as depicted for a PVA chain with the planar zigzag conformation at the top of Figure 1; a larger downfield shift will be induced for the CH carbon I when the OH group chemically bonded to this carbon forms the intramolecular hydrogen bonds with the OH groups on both sides in the *mm* sequence. In contrast, a smaller or no downfield shift may be observed for the CH carbon II or III bonded to the OH groups, which are associated with one or no intramolecular hydrogen bonding in the *mr* and *rr* sequences, respectively. However, the relative intensities of the component lines of the triplet cannot be simply described in terms of the fractions of the *mm*, *mr*, and *rr* sequences even for the spectra of the crystalline and noncrystalline components, which were separately recorded using the difference in ^{13}C spin-lattice relaxation times T_{1c} of the two components.[21] This discordance suggests that the intermolecular hydrogen bonding, which may induce no downfield shift due to the weak deshielding effect,[21] may be formed at a certain probability even in the meso parts in the *mm* and *mr* sequences. In this paper, therefore, we statistically calculate the fractions of the CH carbons associated with the intramolecular and intermolecular hydrogen bondings in the triad sequences and compare them with the relative intensities of the component lines I, II, and III of the CH triplet for PVA samples with different tacticities.

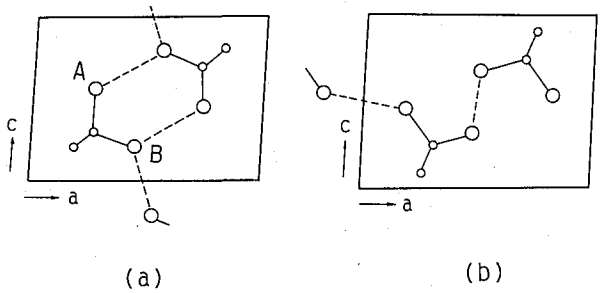

Fig. 2 Crystal structure models (b-projections) proposed by Bunn (a) and Sakurada *et al.* (b).

STATISTICAL CALCULATION

Although the crystal structure of PVA has intensively been studied by many research groups, the detailed structure has not yet been confirmed. In these investigations there is no conflict for a two-molecule monoclinic unit cell with a $\simeq$ 7.83 Å, b $\simeq$ 2.52 Å (fiber axis), c $\simeq$ 5.51 Å, and $\beta \simeq 92°$.[22-25] However, the relative positions of the molecular chains in the b-projection and the hydrogen bonding are still controversial subjects.

Figure 2 shows the projections of the molecular chains to the a-c plane in crystal structure models proposed by Bunn[23] and Sakurada *et al.*,[24] which are regarded as representative models of PVA at present. In both models oxygen atoms, which are drawn as larger circles, are randomly placed in either site of the two possible positions. However, there are significant differences in relative positions of the respective atoms and in the hydrogen bonds depicted by broken lines between these two models. Because of the simplicity of the hydrogen bonding, we adopt here the model proposed by

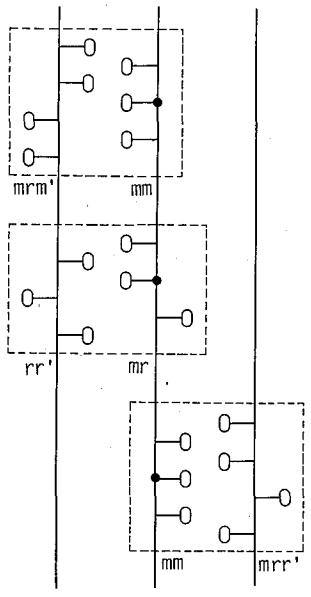

Fig. 3 Triad-tetrad or triad-triad pairs which may form intramolecular and intermolecular hydrogen bonds along three PVA chains in the crystalline region. Closed circles: CH carbons associated with the triplet splitting of the CP/MAS ^{13}C NMR spectrum; O: oxygen atoms.

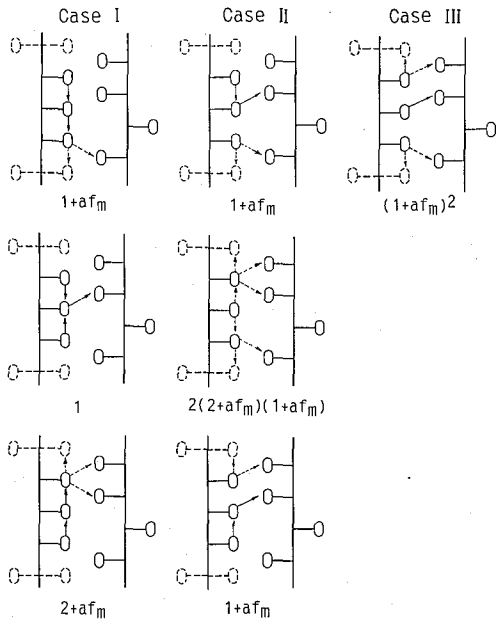

Fig. 4 Intramolecular and intermolecular hydrogen bondings for the *mm-mrr'* pair of PVA.

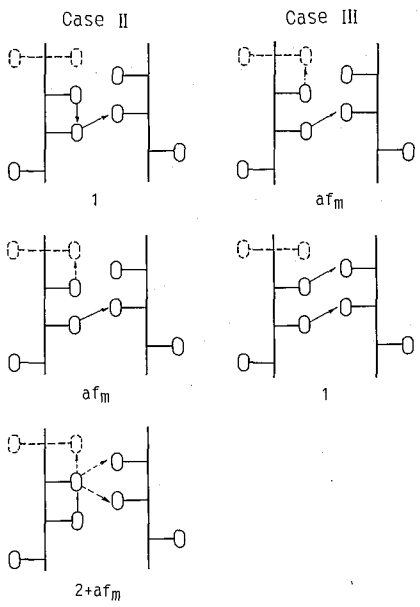

Fig. 5 Intramolecular and intermolecular hydrogen bondings for the *mr-mr* pair of PVA.

Sakurada *et al.* A similar statistical calculation will be also carried out somewhere for Bunn model.

According to the model of Sakurada *et al.* (Figure 2b), one neighboring PVA chain associated with the intermolecular hydrogen bonding with a given PVA chain is placed in the same unit cell or in the neighboring unit cell. The molecular chains connected through the intermolecular hydrogen bonding are shifted with each other by a half of the period (1.26 Å) along the b axis. Accordingly, we focus our attention on the *mm* and *mr* sequences along the central chain shown in Figure 3, and examine the formation of the intramolecular and intermolecular hydrogen bondings for the possible pairs between the triad sequences in the central chain and the tetrad or triad sequences in the neighboring chains. As examples, three pairs of *mm-mrr'*, *mm-mrm'*, and *mr-rr'* are shown in Figure 3. Here, closed circles indicate the CH carbons associated with the triplet of the CP/MAS ^{13}C NMR spectrum of PVA, and each sequence with prime simbols is a mirror image of the corresponding sequence without them.

Figures 4 and 5 show the formation of the intramolecular and intermolecular hydrogen bonds for the *mm-mrr'* and *mr-mr* pairs. Here, cases I, II, and III correspond to the cases where two, one, and no intramolecular hydrogen bond(s) will be formed in the concerned triad sequence, and their fractions are related to the relative intensities of the component lines of the CH triplet in the CP/MAS ^{13}C NMR spectrum as described later. In these figures, each arrow indicates the direction of the OH group and arrows drawn by broken lines indicate the plural possible hydrogen bonds for each OH group. For simplicity, we assume that each OH group in the central chain in question, which corresponds to the left-side chain for each pair shown in Figures 4 and

5, forms either intramolecular or intermolecular hydrogen bond at a certain probability without being influenced by the existence of the OH groups in the neighboring chains. On the other hand, we consider the influence of the OH groups (shown by broken lines) adjacent to the OH groups of the concerned triad sequence in the same chain as follows; only meso-type OH groups of such adjacent groups can form the intramolecular hydrogen bonding with the OH groups located at both ends of the triad sequence in the central chain and the probability of the formation of the intramolecular hydrogen bonding is assumed to be af_m for the latter OH groups. Here, f_m is the fraction of the meso sequence and a is the probability that the H atoms of the adjacent OH groups do not participate in the intramolecular hydrogen bonding in question. Since there are four oxygen atoms associated with an intramolecular or intermolecular hydrogen bond with the adjacent OH group in question, a ranges from 0.75 to 0. In Figures 4 and 5, the number of possible cases is shown for each pair, which is estimated by assuming that the intramolecular and intermolecular hydrogen bonds are formed at an equal probability.

Similar estimations are conducted for all possible triad i-tetrad j or triad i-triad j pairs and the fractions f_{ij}^{I}, f_{ij}^{II}, f_{ij}^{III} of cases I, II, and III are calculated for each i-j pair. Then, the total fractions F_{I}, F_{II}, F_{III} of cases I, II, and III are given by

$$F_{\mathrm{I}}=g_{mm}\sum_j g_j f_{mmj}^{\mathrm{I}} \tag{1}$$

$$F_{\mathrm{II}}=g_{mm}\sum_j g_j f_{mmj}^{\mathrm{II}}+g_{mr}\sum_j g_j f_{mrj}^{\mathrm{II}} \tag{2}$$

$$F_{\mathrm{III}}=g_{mm}\sum_j g_j f_{mmj}^{\mathrm{III}}+g_{mr}\sum_j g_j f_{mmj}^{\mathrm{III}}+g_{rr} \tag{3}$$

where g_{mm}, g_{mr}, *and* g_{rr} are the fractions of the *mm*, *mr*, and *rr* sequences, respectively, and g_j are the fractions of triad or tetrad sequences j. Table 1 files the fractions of f_{ij}^{I}, f_{ij}^{II}, and f_{ij}^{III} calculated for 16 *mm*-tetrad pairs and 8 *mr*-triad pairs by assuming that the probabilities of the intramolecular and intermolecular hydrogen bondings are p_a and p_e ($p_a+p_e=1$), respectively.

On the other hand, the fractions F_a and F_e of the OH groups associated with the intramolecular and intermolecular hydrogen bondings can be also calculated by the following equations, respectively;

$$F_a=g_{mm}\sum_j g_j f_{mmj}^{a}+g_{mr}\sum_j g_j\ f_{mrj}^{a} \tag{4}$$

$$F_e=1-F_a \tag{5}$$

Here, f_{mmj}^{a} and f_{mrj}^{a} are the fractions of the central OH gorups in the *mm* and *mr* sequences which from the intramolecular hydrogen bonds for the *mm*-tetrad j and *mr*-triad j pairs, respectively. Table 2 summarizes f_{ij}^{a}s for the respective i-j pairs.

Table 1 Fractions of Cases I, II, and III for Different Triad-Tetrad and Triad-Triad Pairs

No.	Pair	f_{ij}^{I}	f_{ij}^{II}	f_{ij}^{III}
1	mm-mmm	$p_a^2(3p_e+af_mp_a)/A_j$	$p_a(7p_e^2+6af_mp_ap_e+a^2f_m^2p_a^2)/A_j$	$p_e(p_e+af_mp_a)(2p_e+af_mp_a)/A_j$
2,3	-mmr,$r'mm$	$p_a^2(5p_e+2af_mp_a)/A_j$	$p_a(8p_e^2+10af_mp_ap_e+2a^2f_m^2p_a^2)/A_j$	$p_e(p_e^2+4af_mp_ap_e+2a^2f_m^2p_a^2)/A_j$
4,5	-mrr', $rr'm$	$p_a^2(4p_e+2af_mp_a)/A_j$	$p_a(6p_e^2+8af_mp_ap_e+2a^2f_m^2p_a^2)/A_j$	$p_e(p_e+af_mp_a)^2/A_j$
6,7	-mrm', $m'r'm$	$p_a^2(3p_e+2af_mp_a)/A_j$	$p_a(p_e^2+6af_mp_ap_e+2a^2f_m^2p_a^2)/A_j$	$af_mp_ap_e(p_e+af_mp_a)/A_j$
8,9	-$rr'r$, $r'rr'$	$p_a^2(3p_e+2af_mp_a)/A_j$	$p_a(3p_e^2+6af_mp_ap_e+2a^2f_m^2p_a^2)/A_j$	$af_mp_ap_e(p_e+af_mp_a)/A_j$
10	-$rm'r'$	$p_a^2(p_e+af_mp_a)/A_j$	$p_a(p_e+af_mp_a)^2/A_j$	0
11	-$r'mr$	$p_a^2(2p_e+af_mp_a)/A_j$	$p_a(2p_e^2+4af_mp_ap_e+a^2f_m^2p_a^2)/A_j$	$af_mp_ap_e(p_e+af_mp_a)/A_j$
12,13	-$rm'm'$, $m'm'r'$	$p_a^2(p_e+2af_mp_a)/A_j$	$2af_mp_a^2(p_e+af_mp_a)/A_j$	0
14,15	-$r'rm'$, $m'r'r$	$2p_a^2(p_e+af_mp_a)/A_j$	$2af_mp_a^2(2p_e+af_mp_a)/A_j$	$a^2f_m^2p_a^2p_e/A_j$
16	-$m'm'm'$	$af_mp_a^3/A_j$	$af_m^2p_a^3/A_j$	0
17	mr-mm	0	$p_a(4p_e+af_mp_a)/A_j$	$p_e(3p_e+2af_mp_a)/A_j$
18	-mr	0	$p_a(3p_e+af_mp_a)/A_j$	$p_e(p_e+af_mp_a)/A_j$
19	-rr'	0	$p_a(2p_e+af_mp_a)/A_j$	$p_e(p_e+af_mp_a)/A_j$
20	-$r'm$	0	$p_a(3p_e+af_mp_a)/A_j$	$p_e(p_e+2af_mp_a)/A_j$
21	-rm'	0	1.0	0
22	-$m'r'$	0	$p_a(p_e+af_mp_a)/A_j$	$af_mp_ap_e/A_j$
23	-$r'r$	0	$p_a(2p_e+af_mp_a)/A_j$	$af_mp_ap_e/A_j$
24	-$m'm'$	0	1.0	0

A_j's indicate the sums of the numerators for the respective pairs.

Table 2 Fractions of the OH Groups Associated with the Intramolecular Hydrogen Bonding for Different Triad-Tetrad and Triad-Triad Pairs

No.	Pair	f_{ij}[a]
1	*mm*-*mm*	$p_a[af_mp_a^2(1+af_m)+2p_ap_e(1+2af_m)+4p_e^2]/A_j$
2,3	-*mmr*, *r'mm*	$p_a[2af_mp_a^2(1+af_m)+3p_ap_e(1+2af_m)+4p_e^2]/A_j$
4,5	-*mrr'*, *rr'm*	$p_a[af_mp_a^2(1+af_m)+3p_ap_e(1+2af_m)+4p_e^2]/A_j$
6,7	-*mrm'*, *m'r'm*	$p_a[af_mp_a^2(1+af_m)+p_ap_e(1+2af_m)]/A_j$
8,9	-*rr'r*, *r'rr'*	$2p_a[af_mp_a^2(1+af_m)+p_ap_e(1+2af_m)+p_e^2]/A_j$
10	-*rm'r'*	$p_a[af_mp_a^2(1+af_m)+p_ap_e(1+2af_m)+p_e^2]/A_j$
11	-*r'mr*	$p_a[af_mp_a^2(1+af_m)+p_ap_e(1+2af_m)+p_e^2]/A_j$
12,13	-*rm'm'*, *m'm'r'*	$p_a[2af_mp_a^2(1+af_m)+p_ap_e(1+2af_m)]/A_j$
14,15	-*r'rm'*, *m'm'r'*	$p_a[2af_mp_a^2(1+af_m)+p_ap_e(1+2af_m)]/A_j$
16	-*m'm'm'*	$af_mp_a^3(1+af_m)/A_j$
17	*mr*-*mm*	$p_a(af_mp_a+2p_e)/A_j$
18	-*mr*	$p_a(af_mp_a+2p_e)/A_j$
19	-*rr'*	$p_a(af_mp_a+p_e)/A_j$
20	-*r'm*	$p_a(af_mp_a+p_e)/A_j$
21	-*rm'*	1.0
22	-*m'r'*	$af_mp_a^2$
23	-*r'r*	$p_a(p_e+af_mp_a)/A_j$
24	-*m'm'*	$(1+af_m)/2$

A_j's are the sums of the numerators shown in Table 1 for the respective pairs.

Table 3 Viscosity-Average Molecular Weights and Tacticities for Different PVA Samples.

Sample	$\bar{M}_v$	Triad			Dyad[a]	
		mm	*mr*	*rr*	*m*	*r*
S-PVA	69,960	0.19	0.48	0.33	0.43	0.57
A-PVA	74,800	0.23	0.50	0.27	0.48	0.52
I-PVA	13,200	0.57	0.35	0.08	0.76	0.24

[a] calculated by the least-square method assuming Bernoullian statistics.

EXPERIMENTAL

Samples. PVA films with different tacticities were used in the dried state unless otherwise noted. The viscosity-average molecular weights and tacticities for the samples, which are coded as S-PVA, A-PVA, and I-PVA according to the triad tacticities, are filed in Table 3. The detailed methods for the preparation and characterization of the samples were described in the previous paper.[21]

^{13}C NMR measurements. High-resolution solid-state ^{13}C NMR measurements were

carried out at room temperature on a JEOL JNM-FX200 spectrometer equipped with a JEOL variable temperature/magic angle spinning (VT/MAS) unit under a static magnetic field of 4.7T. ^{1}H and ^{13}C radiofrequency field strengths $\gamma B_1/2\pi$ were 69 kHz for the CP process and in most of pulse sequences used in this work, whereas the ^{1}H field strength was reduced to 59 kHz for the dipolar decoupling process. A cylinder-type MAS rotor with an O-ring seal[10,21] was used for dried and hydrated samples to prevent the absorption of moisture or the loss of water during NMR measurements. The detailed procedure of NMR measurements was almost the same as described in the previous paper.[21]

RESULTS AND DISCUSSION

In Figure 6 the fractions $F_{\rm I}$, $F_{\rm II}$, and $F_{\rm III}$, which were calculated for $p_a=p_e=0.5$ and $a=0.25$ or 0.75 by eqs. (1)-(3), are plotted against the meso fraction f_m. For comparison, the fractions of the *mm*, *mr*, and *rr* sequences, that were estimated from f_m assuming Bernoullian statistics, are also shown as broken lines in this figure. With increasing f_m, the fractions $F_{\rm I}$ and $F_{\rm III}$ more prominently deviate from the fractions of *mm* and *mr* sequences, respectively. In case II, the fraction is almost in accord with the fraction of the *mr* sequence for $f_m<0.5$, but the deviation becomes much enhanced for $f_m>0.5$. These results indicate that the effect of the intermolecular hydrogen bonding, which is formed in the meso parts of the *mm* and *mr* sequences, becomes much clearer for larger f_m values. Moreover, larger a values seem to enhance the discordances between two corresponding fractions mentioned above. This may be related to the terminal effect of the concerned triad; when the a value is increased, the OH groups at both sides of the concerned triad form the intramolecular hydrogen bonding at a higher probability with the oxygen atoms adjacent to these OH groups in the same molecule and this leads to the reduction in the probability of the intramolecular hydrogen bonding in the interior of the triad sequence.

In Figure 7 the fractions $F_{\rm I}$, $F_{\rm II}$, and $F_{\rm III}$ are ploted as a function of p_a for $f_m=0.5$ and $a=0.25$ or 0.75. Interestingly, the fractions $F_{\rm I}$ and $F_{\rm II}$ are considerably high even

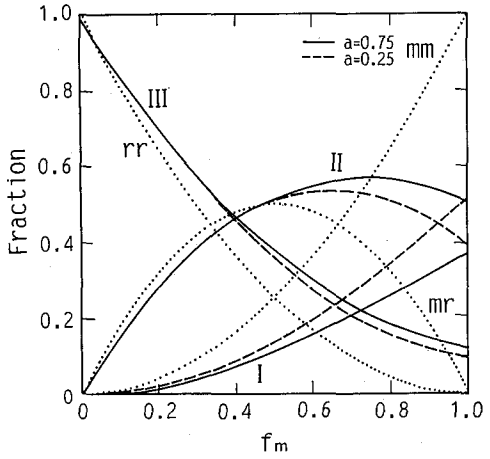

Fig. 6 Dependence of fractions $F_{\rm I}$, $F_{\rm II}$, and $F_{\rm III}$ calculated from eqs. (1)-(3) on f_m; $p_a=0.5$, $a=0.25$ or 0.75. The dotted lines indicate the fractions of the *mm*, *mr*, and *rr* sequences..

for very low p_a values, although those values cannot be calculated for $p_a=0$ by eqs. (1) and (2). This may be due to that some OH groups of the *mm* and *mr* sequences exclusively form the intramolecular hydrogen bonding without any possibility of the intermolecular hydrogen bonding. On the other hand, fractions F_I and F_{III} are gradually increased with increasing p_a, while F_{III} is monotonously decreased. Finally, F_I, F_{II}, and F_{III} tend to approach to the fractions 0.25, 0.50, and 0.25 of the *mm*, *mr*, and *rr* sequences, respectively. This tendency is somewhat more appreciable for a smaller a value, although there seems to be no large difference in fractions F_I, F_{II}, and F_{III} for different a values.

In Figure 8 the fraction F_a of the OH groups associated with the intramolecular hydrogen bonding, which was calculated by eq. (4), is plotted against the fraction f_m for $a=0.5$ and $p_a=0.25$, 0.50, and 0.75. Fraction F_a is almost linearly increased with increasing f_m for the respective p_a values and, as is expected, a higher p_a value gives a higher F_a for each f_m. In this case there was also no large difference in F_a for different a values.

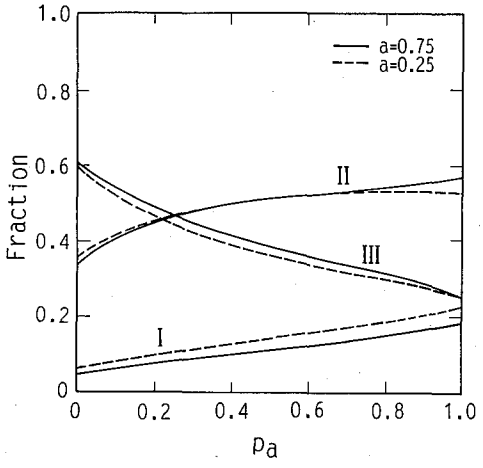

Fig. 7 Dependence of fractions F_I, F_{II}, and F_{III} calculated from eqs. (1)-(3) on p_a; $f_m=0.5$, $a=0.25$ or 0.75.

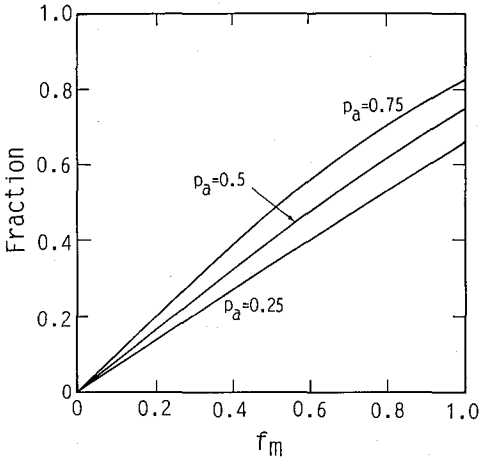

Fig. 8 Dependence of fraction F_a calculated from eq.(4) on f_m for different p_a values with $a=0.5$.

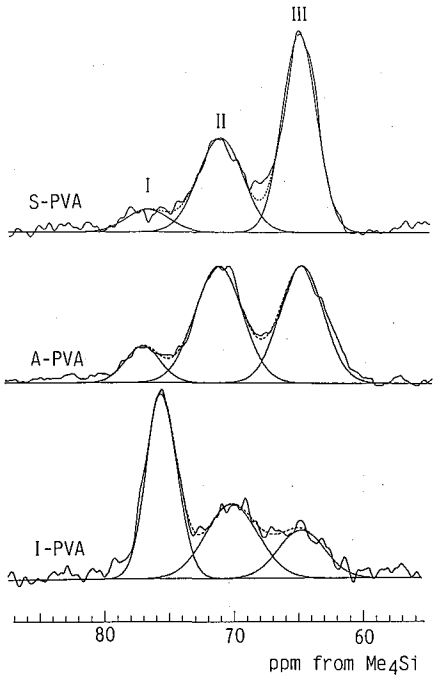

Fig. 9 Lineshape analyses of the CH triplets of the crystalline components of different PVA samples.

As described in the previous paper,[21] we measured CP/MAS ^{13}C NMR spectra of the crystalline and noncrystalline components of PVA films with different tacticities and determined the relative intensities of the CH triplets by the lineshape analyses. Figure 9 shows the results of the lineshape analyses for the CH resonance lines of the crystalline components of dry S-PVA, A-PVA, and I-PVA, which were measured by the CPT1 pulse sequence[26] at room temperature. Here, each line was assumed to be described as a Gausssian.

Table 4 files the integrated fractions of lines I, II, and III of the CH triads obtained for different PVA films by the lineshape analyses. In this table the calculated fractions $F_{\rm I}$, $F_{\rm II}$, and $F_{\rm III}$ of the corresponding CH carbons, which were obtained from eqs. (1)-(3) using the least-square method so as to fit them with the observed fractions, are also shown together with p_a and F_a values. Here, the a value was assumed to be 0.5 in every case, because this value is close to the arithmetic average of possible a values. The calculated fractions fairly well agree with the observed ones except for I-PVA. Interestingly, the probability p_a of the intramolecular hydrogen bonding for the crystalline component is much less for S-PVA than for A-PVA, although the difference in meso content is only 0.05 between these two samples as seen in Table 3. This suggests that the intermolecular hydrogen bonding may be preferentially formed for samples with the f_m value less than some threshold value. In contrast, for the almost atactic PVA (A-PVA) there is no large difference in probabilities of the intramolecular and intermolecular hydrogen bondings; $p_a=0.32$ and $p_e=0.68$. In I-PVA, however, the accordance between the two fractions is not so good. This may be due to that p_a depends on the sort of i-j pairs particularly for the samples with higher isotacticities. For example, p_a may be high for mm-$m'm'r'$ pair in the mm-rich two chains where

Table 4 Observed and Calculated Fractions of the CH Carbons I, II, and III for Different PVA Samples.

Sample	Observed fraction			Calculated fraction			p_a[a]	F_a[b]
	I	II	III	I	II	III		
Crystalline								
S-PVA	0.064	0.350	0.586	0.048	0.364	0.588	0.08	0.239
A-PVA	0.109	0.457	0.434	0.090	0.473	0.437	0.32	0.343
A-PVA, hydrated[c]	0.154	0.513	0.333	0.143	0.522	0.335	0.74	0.455
I-PVA	0.386	0.351	0.263	0.368	0.519	0.113	0.89	0.744
Noncrystalline								
A-PVA	0.170	0.493	0.337	0.147	0.524	0.329	0.77	0.467

[a] Probability of the intramolecular hydrogen bonding. [b] Fraction of OH groups associated with the intramolecular hydrogen bonding, which was calculated according to eq.(4). [c] The water content is 18% as described by (g H_2O/g PVA)×100%.

almost all OH groups are located at the opposite sites with each other. In contrast, when these OH groups in the two chains are placed at the same side, p_a should become low, for example, for *mm-mmr* pair.

On the other hand, the fractions of CH carbons I and II increase by about 0.05 for the crystalline component of hydrated A-PVA compared to those for dried A-PVA. According to the statistical calculation above mentioned, this change is induced by the increase of p_a from 0.32 to 0.74 upon the absorption of water. The x-ray crystal structure analysis revealed that water does not change the crystal lattice of PVA.[27] However, ^{13}C spin-lattice relaxation times of the CH and CH_2 carbons for the crystalline component of A-PVA are significantly decreased by the addition of water.[20,21] Accordingly, a small amount of water, which is not enough to expand the crystal lattice, must diffuse into the crystalline region and break exclusively the intermolecular hydrogen bonding. As a result, new intramolecular hydrogen bonds will be produced in the *mm*, and *mr* sequences, leading to the increase in F_{I} and F_{II}. This change may also allow the enhancement in molecular mobility of PVA chains in the crystalline region.

As for the noncrystalline component of dry A-PVA, the observed fractions of the CH carbons are very close to those for the crystlline component of hydrated A-PVA. This may suggest that the local structure of PVA chains in the noncrystalline region is almost the same as that in the crystalline region as long as it is examined through the hydrogen bonding in the triad sequence. Nevertheless, there must be some freedom for OH groups to form the intramolecular hydrogen bonding at higher probability (p_a= 0.74) even in the dried state possibly because of the higher molecular mobility in the noncrystalline region.

Finally, we briefly discuss about the results expected when we adopt Bunn model. There are also two sites, A and B, for each oxygen atom in this model (Figure 2(a)) but one of these (site B) is associated with two intermolecular hydrogen bonds as indicated by broken lines in this figure. In site B, therefore, we must elucidate the intramolecular and intermolecular hydrogen bondings between the central chain and two neighboring

chains, whereas the same threatment is possible in site A as for the case of the model of Sakurada *et al.* The increase of the number of the neighboring chains should result in the increase of the fractions of the intermolecular hydrogen bonds if the probabilities of the respective hydrogen bondings stay constant. This will lead to the reduction in fractions F_{I} and F_{II}. Accordingly, p_a values should be increased in Bunn model compared to the case of the model of Sakurada *et al.* if the good fit with the observed fractions is expected. More detailed discussion will be described somewhere after the statistical calculation is carried out using Bunn model.

REFERENCES

(1) R. Kitamaru, F. Horii, and K. Murayama, *Macromolecules,* **19**, 636 (1986).
(2) M. Nakagawa, F. Horii, and R. Kitamaru, *Polymer,* **31**, 323 (1990).
(3) T. Kimura, K. Neki, N. Tamura, F. Horii, M. Nakagawa, and H. Odani, *Polymer*, in press.
(4) Q. R. Zhu, F. Horii, M. Tsuji, and R. Kitamaru, *J. Soc. Rheology, Japan,* **17**, 35 (1989).
(5) R. Kitamaru, F. Horii, Q. R. Zhu, D. C. Bassett, and R. H. Olley, *Polym. Prepr., Japan,* **D37**, 2609 (1988); to be submitted to *Polymer.*
(6) S. Saito, Y. Moteki, M. Nakagawa, F. Horii, and R. Kitamaru, *Macromolecules,* **23**, 3256 (1990).
(7) A. Hirai, F. Horii, R. Kitamaru, J. G. Fatou, and A. Bello, *Macromolecules,* **23**, 2913 (1990).
(8) F. Horii, In "Nuclear Magnetic Resonance in Agriculture," P. E. Pfeffer and W. V. Gerasimowicz, Ed., CRC Press, Florida, 1989, Chapter 10.
(9) H. Yamamoto, F. Horii, and H. Odani, *Macromolecules,* **22**, 4130 (1989).
(10) F. Horii, H. Yamamoto, A. Hirai, and R. Kitamaru, In "Cellulose: Structural and Functional Aspects," J. F. Kennedy, G. O. Phillips, and P. A. William, Ed., Ellis Horwood, Chichester, 1990, p.125.
(11) J. Sugiyama, T. Okano, H. Yamamoto, and F. Horii, *Macromolecules,* **23**, 3196 (1990).
(12) A. Hirai, F. Horii, R. Kitamaru, and W. Tsuji, *J. Polym. Sci. Part C: Polym. Lett.*, 28, 357 (1990).
(13) F. Horii, H. Yamamoto, A. Hirai, and R. Kitamaru, *Carbohyd. Res.*, **160**, 29 (1987).
(14) A. Hirai, T. Ito, F. Horii, R. Kitamaru, K. Kobayashi, and H. Sumitomo, *Macromolecules,* **23**, 1837 (1990).
(15) F. Horii, Y.-Y. Chen, M. Nakagawa, B. Gabrys, and R. Kitamaru, *Bull. Inst. Chem. Res., Kyoto Univ.*, **66**, 317 (1988).
(16) F. Horii, A. Hirai, K. Murayama, R. Kitamaru, and T. Suzuki, *Macromolecules,***16**,273 (1983).
(17) T. Murata, F. Horii, and H. Odani, *Polym. Prepr., Japan,* **39**, 1055 (1990).
(18) T. Uyeda, F. Horii, H. Odani, T. Masuda, and T. Higashimura, *Polym. Prepr., Japan,* **40**, 113 (1991).
(19) T. Terao, S. Maeda, and A. Saika, *Macromolecules,* **16**, 1535 (1983).
(20) F. Horii, T. Ito, and R. Kitamaru, *ACS Polym. Prepr.*, **29**, No.1, 27 (1988).
(21) F. Horii, S. Hu, T. Ito, H. Odani, R. Kitamaru, S. Matsuzawa, and K. Yamaura, *Polymer*, in press.
(22) R. C. L. Mooney, *J. Am. Chem. Soc.*, **63**, 2828 (1941).
(23) C. W. Bunn, *Nature,* **161**, 929 (1948).
(24) I. Sakurada, K. Futino, and A. Okada, *Bull. Inst. Chem. Res., Kyoto Univ.*, **23**, 78 (1950).
(25) I. Nitta, I. Taguchi, and Y. Chatani, *Ann. Rep. Inst. Fiber Sci.*, **10**, 1 (1957).
(26) D. A. Torchia, *J. Magn. Reson.*, **44**, 117 (1981).
(27) I. Sakurada, Y. Nukushina, and Y. Sone, *Kobunshi Kagaku,* **12**, 510 (1955).